Two-dimensional nonuniformly heated magnetized plasma transport in a conducting vessel

L. L. Beilinson, V. A. Rozhansky, and L. D. Tsendin
Physical-Technical Department, St. Petersburg State Technical University, St. Petersburg 195251, Russia
(Received 24 January 1994)

The model of a cylindrical, axially symmetric discharge with conducting walls in a uniform axial magnetic field is considered. An analytic method which can be used for a wide range of conditions is suggested. The results agree with the full-scale numerical modeling [IEEE Trans. Plasma Sci. **PS-19**, 204 (1991)]. It is shown that a possibility exists to control the discharge parameters by applying a potential difference to the sectioned vessel walls.

PACS number(s): 52.25.Fi

I. INTRODUCTION

The problem of a magnetized nonisothermal plasma transport in a conducting vessel is of considerable interest in connection with the numerous applications of rf discharges in the magnetic fields in plasma surface processing. The complete problem of gas discharge modeling consists of (a) description of rf wave propagation and absorption in inhomogeneous plasma, which is a source an energy input into discharge; (b) analysis of the formation of an electron distribution in inhomogeneous RF and stationary fields, which is responsible for the ionization processes; and (c) analysis of charged particle transport and their loss from the plasma volume.

Each of these parts is rather complicated. Full-scale numerical modeling of the transport problem for several simple plasma configurations was performed in [1]. In that paper a given energy input profile and Maxwellian electron distribution function were postulated. The ion motion was described by the Monte Carlo simulation. The discharge volume was not separated into the quasineutral plasma and the space-charge sheath, and the Poisson equation was solved over the whole volume. The resulting calculations turned out to be very labor consuming and could be performed only by a supercomputer. This implies that self-consistent modeling of the whole discharge with such accuracy by means of modern computer techniques is an extremely difficult task. It is worthwhile to mention that such numerical modeling has no predictive power and only an analytic solution enables one to deduce the dependencies of the plasma properties on external parameters such as current, pressure, magnetic field intensity, discharge geometry, properties of the vessel walls, etc.

The analytic approach to such problems based on the simple fluid equations in the quasineutral approximation was developed in [2–4] for Simon's short-circuiting problem [5] in the isothermal magnetized plasma. Several more complicated problems with nonuniform electron temperature profiles were also treated in [6] numerically. We shall demonstrate here that the analytic approach can be easily generalized for the nonisothermal plasma and nonequipotential boundary. If an ion free path λ_i is small compared to the discharge length L, the fluid approximation is applicable. It is shown that all the principal results of [1] are easily reproduced and their physical meaning can be clarified. The account of the finite value of λ_i/L is performed in the framework of a kinetic description of the ion motion. This considerably improves the quantitative agreement of the analytic results with the calculations [1]. The applying of the potential difference to various parts of the vessel walls enables one to control the profiles of plasma parameters and particles and energy fluxes to the surface.

II. PLASMA TRANSPORT FOR THE FIXED $T_e(r)$ PROFILE

We consider here the nonisothermal plasma with the given $T_e(r)$ profile, in a conducting cylindrical vessel of length L and radius R immersed in a stationary uniform magnetic field $\vec{B}=B_z$ parallel to the cylinder axis. We restrict ourselves to the axially symmetric problem with the collision-dominated ion motion. Only the case of monotonic temperature profile with the maximal value of $T_e(r)$ at $r=0$ [1] and Maxwellian electron distribution are considered. The electron mobility across z is strongly suppressed by the magnetic field. Such approximation is valid if

$$b_{e\perp} \ll b_{i\perp} , \tag{1a}$$

where $b_{i\perp}, b_{e\perp}$ are the ion and electron mobilities across the magnetic field. This inequality is equivalent to

$$\omega_{ce}\omega_{ci} \gg \nu_{ea}\nu_{ia} ,$$

where $\omega_{ce,ci}$ are cyclotron frequencies and $\nu_{ea,ci}$ are transport collision frequencies of charged with neutral particles. The electrons are electrostatically trapped in the longitudinal direction when

$$\tau_{e\parallel} = \frac{(L/\pi)^2}{D_{e\parallel}} \ll \frac{(R/2.4)^2}{D_{i\perp}(1+T_e/T_i)} = \tau_{i\perp} , \tag{1b}$$

where $D_{e\parallel}$ and $D_{i\perp}$ are electron and ion diffusion coefficients along and across the magnetic field [4]. Longitudinal electron thermal conductivity and diffusion coefficients are large compared to the ion ones, so the electron temperature should be independent of z. Since

 ©1994 The American Physical Society

the electrons are trapped up along $\vec{B}$, they should have the Maxwell-Boltzmann distribution (this is also valid for the collisionless case):

$$\varphi(r,z)=\frac{T_e(r)}{e}\ln[n(r,z)/n_m(r)]+\varphi_m(r) , \tag{2}$$

where n_m,φ_m are the maximal values of the plasma density and potential at a given radius. For the collisionless sheath along $\vec{B}$ the longitudinal electron flux at the end wall $\Gamma_{e\|s}$ is determined by the potential difference in the sheath $\Delta\varphi$:

$$\Gamma_{e\|s}(r)=1/(2\pi)^{1/2}n_b[T_e(r)/m_e]^{1/2}\exp[-e\Delta\varphi/T_e(r)] , \tag{3}$$

where n_b is the plasma density at the sheath edge. For further details, see [4], where formulas for the collision-dominated sheath and for the non-Maxwellian electrons are also derived. Equation (2) is valid for $n\geq n_b$. By combining Eqs. (2) and (3), we obtain the potential profile in a plasma with respect to the conducting equipotential end walls:

$$\varphi(r,z)=\frac{T_e(r)}{e}\ln\left[\frac{n(r,z)[T_e(r)/m_e]^{1/2}}{(2\pi)^{1/2}\Gamma_{e\|s}(r)}\right] . \tag{4}$$

As we have neglected the transverse electron transport, the flux $\Gamma_{e\|s}(r)$ is determined by the ionization frequency $\nu_i(T_e(r))$:

$$2\Gamma_{e\|s}(r)=\nu_i(T_e(r))\int_0^L n(r,z)dz . \tag{5}$$

For the Maxwellian electrons in argon, the approximate expression for $\nu_i(r)$ is given by

$$\nu_i(r)=N_a\sigma_{i0}[8T_e(r)/\pi m_e]^{1/2}\exp[-\varepsilon/T_e(r)] , \tag{6}$$

where N_a is the density of the neutral particles and σ_{i0} and ε are the adjustment constants ($\varepsilon=16.3$ eV, $\sigma_{i0}=3.1\times10^{-16}$ cm^2) [1]. Substituting Eq. (6) into Eq. (4), we obtain

$$\varphi(r,z)=\varepsilon/e+\alpha(r,z)T_e(r)/e , \tag{7}$$

where

$$\alpha(r,z)=\ln\left\{n(r,z)\Big/\left[(2LN_a\sigma_{i0})\int_0^L n(r,z)dz\right]\right\} . \tag{8}$$

Equations (7) and (8) express the potential in the plasma in terms of the density and $T_e(r)$ profiles and enable one to obtain an analytic solution of the problem. If the density profile can be factorized as $n=f_1(z)f_2(r)$, the value of α is r independent. For example, if $f_1(z)=\sin(\pi z/L)$, we have

$$\alpha=\alpha(z)=\ln\left[\frac{\pi\sin(\pi z/L)}{4LN_a\sigma_{i0}}\right] .$$

The value of α can be both negative or positive. We restrict ourselves to the case of positive α. With the potential given by Eq. (7), one can solve the ion transport equation. In the stationary case it has the form

$$\frac{1}{r}\frac{\partial}{\partial r}\left[r\left[D_{i\perp}\frac{\partial n}{\partial r}+b_{i\perp}n\frac{\partial\varphi}{\partial r}\right]\right]+\frac{\partial}{\partial z}\left[D_{i\|}\frac{\partial n}{\partial z}+b_{i\|}n\frac{\partial\varphi}{\partial z}\right]+\nu_i(T_e(r))n=0 . \tag{9}$$

From Eq. (9) the physical reason for the distinction between the cases of uniform and nonuniform $T_e(r)$ profiles is clearly seen. If $T_e(r)=$const, the radial electric field is determined, according to Eqs. (7) and (8), only by the slow logarithmic dependence of $\alpha(r)$. The radial ion transport [the first term in the left-hand side of (9)] is connected with this small electric field and with the radial ion diffusion. In the opposite case, as the ion temperature $T_i\ll T_e$ and the potential equation (7) is determined by T_e, it is possible to neglect the ion diffusion terms in Eq. (9). Substituting Eq. (7) into Eq. (9), we have

$$\frac{1}{r}\frac{\partial}{\partial r}\left[r\left[\frac{b_{i\perp}}{e}n\frac{\partial(\alpha T_e)}{\partial r}\right]\right]+\frac{b_{i\|}T_e(r)}{e}\frac{\partial^2 n}{\partial z^2}+\nu_i n=0 . \tag{10}$$

Neglecting the weak logarithmic dependence $\alpha(r,z)\approx\bar{\alpha}$, it is possible to seek the solution in the form

$$n=n_m(L/2,0)f_1(z)f_2(r) . \tag{11}$$

Employing Eq. (10), one obtains

$$\frac{\frac{b_{i\perp}}{e}\frac{1}{r}\frac{\partial}{\partial r}\left[rf_2\frac{\partial T_e}{\partial r}\right]}{T_e f_2}+\frac{\frac{b_{i\|}}{e}\frac{\partial^2 f_1}{\partial z^2}}{\bar{\alpha}f_1}=-\frac{\nu_i(T_e)}{T_e\bar{\alpha}} . \tag{12}$$

The second term in the left-hand side is the only z-dependent one. So it is equal to the constant C_1. The equations for f_1,f_2 are given by

$$\frac{b_{i\|}}{e}\frac{\partial^2 f_1}{\partial z^2}=C_1\bar{\alpha}f_1 , \tag{13}$$

$$\left[\frac{b_{i\|}}{e}\frac{1}{r}\frac{\partial}{\partial r}\left[rf_2\frac{\partial T_e}{\partial r}\right]\right]\Big/(T_e f_2)=-\frac{\nu_i(T_e)}{T_e\bar{\alpha}}-C_1 . \tag{14}$$

From the boundary condition $f_1(z=0,L)=0$, it follows that

$$f_1=\sin(\pi z/L),\quad C_1=-\frac{b_{i\|}}{\bar{\alpha}e}\left[\frac{\pi}{L}\right]^{1/2} . \tag{15}$$

Substituting Eq. (15) into Eq. (14), one obtains

$$\bar{\alpha}\frac{b_{i\|}}{e}\frac{1}{r}\frac{\partial}{\partial r}\left[rf_2\frac{\partial T_e}{\partial r}\right]=[-\nu_i(T_e)+\tau_{a\|}^{-1}]f_2 , \tag{16}$$

where

$$\tau_{a\|}^{-1}=\frac{T_e}{e}b_{i\|}\left[\frac{\pi}{L}\right]^2=D_{a\|}\left[\frac{\pi}{L}\right]^2$$

is the inverse time of the longitudinal ambipolar

diffusion. The solution of Eq. (16) for an arbitrary $T_e(r)$ profile is given by

$$f_2=\exp\left[-\int_0^r \frac{\beta(r')+j(r')}{\frac{b_{i\perp}\bar{\alpha}}{e}\frac{\partial T_e}{\partial r'}}dr'\right], \quad (17)$$

where $\beta(r)=\nu_i(T_e)-\tau_{a\parallel}^{-1}$ and

$$j(r)=\frac{\bar{\alpha}b_{i\perp}}{e}\frac{1}{r}\frac{\partial}{\partial r}\left[r\frac{\partial T_e}{\partial r}\right].$$

The $\bar{\alpha}$ value can be replaced approximately by

$$\alpha(0)=\ln\frac{\pi}{4LN_a\sigma_{i0}}. \quad (18)$$

Plasma density is finite in the vessel center, where $(\partial T_e/\partial r)|_{r=0}=0$. So $\beta(0)+j(0)=0$. As

$$j(0)=2\frac{\bar{\alpha}b_{i\perp}}{e}\frac{\partial^2 T_e}{\partial r^2}\bigg|_{r=0},$$

we obtain the equation for the central electron temperature T_{em},

$$\nu_i(T_{em})-\frac{T_{em}\pi^2}{m_i\nu_{ia}L^2}+\frac{2\bar{\alpha}b_{i\perp}}{e}\frac{\partial^2 T_e}{\partial r^2}\bigg|_{r=0}=0, \quad (19)$$

where the ionization rate is given by Eq. (6).

Equation (19) describes the one-dimensional balance between generation and longitudinal diffusion of the electrons. For the arbitrary $T_e(r)$ profile, the value of T_{em} is larger than for $T_e=$const, if $\bar{\alpha}>0$ (such a situation was considered in [1]), because $(\partial^2 T_e/\partial r^2)|_{r=0}<0$. This means that the ion generation at $r=0$ is now compensated by their diffusion along z as well as by the radial outward convection. (Note that for a vessel long enough, $\bar{\alpha}$ is negative. A more complicated situation such as this is beyond our consideration now.)

It should be particularly emphasized that all the main results presented in this section follow from Eqs. (2), (3), and (6), which are based on the assumption of the Maxwellian electron distribution function. But the electron losses on the vessel walls and inelastic electron-neutral collisions (e.g., excitation and ionization) result in considerable depletion of the electron distribution tail and reduce the values of $\Gamma_{e\parallel s}$ and ν_i with respect to Eqs. (3) and (6). These expressions are valid only in relatively highly ionized plasma, when the electron-electron collisions are frequent enough to restore the Maxwellian distribution. In the opposite case, the whole problem becomes of essentially kinetic nature, and the radial potential profile is determined by the form of the electron distribution function tail [7].

III. ENERGY BALANCE

The profile of $T_e(r)$ is determined by the electron energy balance equation averaged over z for the given profile of power input $P(r)$:

$$P(r)=\int_0^L \rho n\,dz=\int_0^L \nu_i n(\varepsilon+3/2T_e)dz-\int_0^L e\Gamma_{e\parallel}\frac{\partial\varphi}{\partial z}dz+4\Gamma_{e\parallel s}T_e, \quad (20)$$

where $\rho(r,z)$ is the power input per one electron. Here the first term in the right-hand side represents the energy losses for the ionization and heating; the second term is the energy which is transferred from the electrons to the ions by means of the longitudinal electric field, Eq. (7); and the last term is the heat flux to the end wall. Employing Eq. (7), the second term can be rewritten in the form

$$-\int e\Gamma_{e\parallel}\frac{\partial\varphi}{\partial z}dz=e\int\varphi\frac{\partial\Gamma_{i\parallel}}{\partial z}dz=\int(\varepsilon+\bar{\alpha}T_e)\frac{\partial\Gamma_{i\parallel}}{\partial z}dz=2(\varepsilon+\bar{\alpha}T_e)\Gamma_{i\parallel s}. \quad (21)$$

Here we have replaced α be $\bar{\alpha}$ because of its slow logarithmic variation. From Eqs. (5), (20), and (21), one obtains finally

$$\rho(r)=\nu_i[2\varepsilon+(\bar{\alpha}+\tfrac{7}{2})T_e]. \quad (22)$$

The energy input profile is determined by the form of the electron distribution function tail. Taking into account the expression for ν_i, Eq. (6), one can obtain $T_e''(0)$ from Eq. (22) as a function of $\rho''(0)$:

$$\frac{\rho''(0)}{\rho(0)}=\frac{T_e''(0)}{T_{em}}\left[\frac{\varepsilon}{T_{em}}+\frac{1}{2}+\frac{\bar{\alpha}+\frac{7}{2}}{(2\varepsilon/T_{em}+\bar{\alpha}+\frac{7}{2})}\right]. \quad (23)$$

Finally, substituting Eq. (23) into Eq. (18), we have the equation for T_{em}:

$$\exp(\varepsilon/T_{em})T_{em}^{1/2}=\frac{2\sqrt{2}m_i\nu_{ia}N_a\sigma_{i0}L^2}{m_e^{1/2}\pi^{5/2}\left\{\frac{b_{i\perp}2\bar{\alpha}L^2}{b_{i\parallel}\pi^2}\frac{\rho''(0)}{\rho(0)A}+1\right\}}, \quad (24)$$

where

$$A=\frac{\varepsilon}{T_{em}}+\frac{1}{2}+\frac{\bar{\alpha}+\frac{7}{2}}{(2\varepsilon/T_{em}+\bar{\alpha}+\frac{7}{2})}.$$

The maximal temperature in the vessel T_{em} is given by Eq. (24), the temperature profile for the arbitrary power deposition is determined by Eq. (22), and the density profile is described by Eqs. (11), (15), and (17). The potential profile is given by Eqs. (7) and (8). These expressions are valid for the plasma parameters when the ion mean free path is small compared to the characteristic system length. For example, for the parameters set

$$\rho(r)=\text{const},\quad N_a=1.2\times10^{13}\text{ cm},\quad L=30\text{ cm},$$

$$\sigma_{i0}=3.1\times10^{-16}\text{ cm},\quad \nu_{ia}=7.0\times10^4,$$

$$\varepsilon=16.3\text{ eV},$$

we obtain from Eq. (24) the value $T_{em}=4.8$ eV, while the simulation [1] gives $T_{em}=3.65$ eV. The difference cannot be attributed to the accuracy of the simulation. It is caused by the fact that under conditions [1], the ion mean free path

$$\lambda_i=(2T_{em}/m_i)^{1/2}/\nu_{ia}\approx 6 \text{ cm} \tag{25}$$

is of the same order as $L/2=15$ cm. In order to develop a more exact approximation, we should use the kinetic equation for ions.

IV. KINETIC METHOD

We start with the simplest case $T_e(r)=\text{const}$. The Maxwell-Boltzmann equation (2) remains valid, as it is based on the distribution of the trapped electrons. In the calculations [1] charge-exchange collisions dominate, and the frequencies of elastic and charge exchange collisions are equal to 30 and 40 kHz, respectively. To simplify calculations, we consider all collisions as charge-exchange ones and take charge-exchange frequency $\nu_{ex}=70$ kHz. The ions are magnetized, and the radial electric field is absent. Therefore, the ion motion can be described by a one-dimensional equation, and f_i depends on v_r, r parametrically. So we obtain the ion kinetic equation

$$v_z\frac{\partial f_i}{\partial z}+\frac{eE_z}{m_i}\frac{\partial f_i}{\partial v_z}=-\nu_{ex}f_i+(\nu_i+\nu_{ex})n(r,z)\delta(v_z)\ . \tag{26}$$

The last term corresponds to the generation of particles in point z with zero velocity. Substituting Eq. (7) in Eq. (26), we have

$$v_z\frac{\partial f_i}{\partial z}+\frac{eE_z}{m_i}\frac{\partial f_i}{\partial v_z}=-\nu_{ex}f_i+(\nu_i+\nu_{ex})n_m(r)\times\exp[-e\varphi(z)/T_{em}]\delta(v_z)\ .$$

Introducing a new variable instead of v_z:

$$\varepsilon=m_iv_z^2/2+e\varphi(z)\ , \tag{27}$$

we obtain Eq. (26) in the form

$$\left[\frac{2}{m_i}\{\varepsilon-e\varphi(z)\}\right]^{1/2}\frac{\partial f_i}{\partial z}=-\nu_{ex}f_i+(\nu_i+\nu_{ex})n(r,z)\times[\varepsilon-e\varphi(z)]^{1/2}\sqrt{m_i/2}\ .$$

Transforming the δ function, we obtain the equation for f_i:

$$\frac{\partial f_i}{\partial z}=\frac{-\nu_{ex}}{\left[\frac{2}{m_i}\{\varepsilon-e\varphi(z)\}\right]^{1/2}}f_i+m_i(\nu_i+\nu_{ex})n_m(r)\exp\left[-\frac{e\varphi(z(\varepsilon))}{T_{em}}\right]\times\delta[z-z(\varepsilon)]/eE[z(\varepsilon)]\ , \tag{28}$$

where $e\varphi(z(\varepsilon))=\varepsilon$. The solution of Eq. (28) is

$$f_i(\varepsilon,z)=\frac{n_m(r)m_i(\nu_i+\nu_{ex})\exp\left[-\frac{e\varphi(z(\varepsilon))}{T_{em}}\right]}{eE[z(\varepsilon)]}\times\exp\left[-\int_{z(\varepsilon)}^{z}\frac{\nu_{ex}dz}{\left[\frac{2}{m_i}\{\varepsilon-e\varphi(z)\}\right]^{1/2}}\right]\ . \tag{29}$$

With this ion distribution function, we can express the ion flux along $\vec{B}$ as a function of z:

$$\Gamma_{i\parallel}(r,z)=\int_0^\infty f_i(v_z,r,z)v_zdv_z=\tfrac{1}{2}\int_0^\infty f_id(v_z^2)=\int_0^\infty f_id\left[\frac{1}{m_i}[\varepsilon-e\varphi(z(\varepsilon))]\right]=n_m(r)\int_0^z(\nu_i+\nu_{ex})\exp\left[-\frac{e\varphi(z')}{T_{em}}\right]\exp\left[-\int_{z'}^{z}\frac{\nu_{ex}dz''}{\left[\frac{2e}{m_i}[\varphi(z')-\varphi(z'')]\right]^{1/2}}\right]dz'\ . \tag{30}$$

The equivalent expression of $\Gamma_{i\parallel}(r,z)$ can be obtained by integrating of Eq. (26) over v_z:

$$\Gamma_{i\parallel}(r,z)=\nu_i(T_{em})n_m(r)\int_0^L\exp\left[-\frac{e\varphi(z')}{T_{em}}\right]dz'\ . \tag{31}$$

Expression (31) means that the ion flux at z is formed by the particles that are generated between 0 and z. By equating Eqs. (30) and (31), we obtain an integral equation for the potential profile $\varphi(z)$. Introducing a new variable and a new function instead of z,φ:

$$Z=[\nu_{ex}/(2T_{em}/m_i)^{1/2}]z,\quad \eta(Z)=\frac{e\varphi(z)}{T_{em}}\ , \tag{32}$$

we obtain the equation for η:

$$(\nu_i+\nu_{ex})\int_0^Z e^{-\eta(Z')}\exp\left[-\int_{Z'}^Z \frac{dZ''}{[\eta(Z'')-\eta(Z')]^{1/2}}\right]dZ' = \nu_i\int_0^Z e^{-\eta(Z')}dZ' \ . \quad (33)$$

Introducing

$$\mu=(\nu_i+\nu_{ex})/\nu_i \ , \quad (34)$$

we have

$$\int_0^Z e^{-\eta(Z')}dZ' = \mu\int_0^Z e^{-\eta(Z')} \times\exp\left[-\int_{Z'}^Z \frac{dZ''}{[\eta(Z'')-\eta(Z')]^{1/2}}\right]dZ' \ . \quad (35)$$

We can obtain $\eta(Z)$ for each value $\mu>1$ by solving Eq. (35) by means of the method stated below. Several curves $\eta(Z)$ corresponding to different values of μ are shown in Fig. 1. All the curves contain the critical point Z_{cr}, so that

$$\left.\frac{\partial\eta}{\partial z}\right|_{z=Z_{cr}} = \infty \ .$$

This point corresponds to the plasma-sheath boundary. As the sheath is thin compared to L, $Z_{cr}(\mu)$ can be identified with the wall coordinate

$$Z_{cr}=L/2[\nu_{ex}/(2T_{em}/m_i)^{1/2}] \ .$$

Thus we have a connection between μ, T_{em}, and L. Dependence of Z_{cr} on μ is shown in Fig. 2. Using simultaneously Fig. 2, Eq. (34), and Eq. (32), we can obtain T_{em} for each value of L. Combining Fig. 2 with Eqs. (32) and (34), we obtain $T_{em}=3.9$ eV, while simulation [1] gives $T_{em}=3.65$ eV. The agreement is reasonable. The difference can be attributed to the accuracy of the simulation.

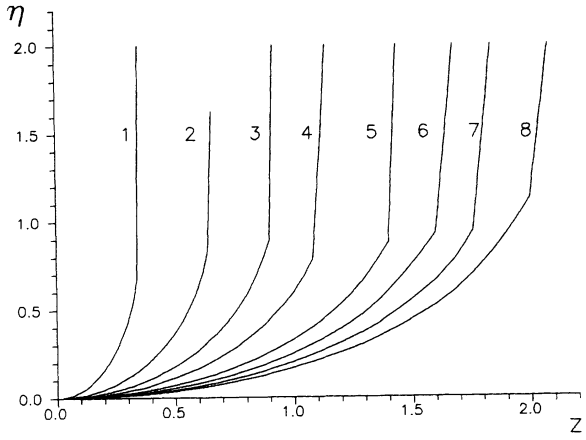

FIG. 1. Solutions of Eq. (35) at different values of μ. Curve 1 corresponds to $\mu=2.0$, curve 2 to $\mu=3.0$, curve 3 to $\mu=4.0$, curve 4 to $\mu=5.0$, curve 5 to $\mu=6.5$, curve 6 to $\mu=7.5$, curve 7 to $\mu=8.5$, curve 8 to $\mu=9.5$, and η and Z are in dimensionless units.

V. GENERALIZATION OF THE KINETIC METHOD FOR THE CASE OF ARBITRARY TEMPERATURE PROFILE

Since the ion Larmor radius is small compared to R, the radial ion transport is also small with respect to the longitudinal one. Accordingly, we shall describe it in the fluid approximation [Eq. (10)]:

$$\Gamma_{i\parallel}(r,z)=[\nu_i(T_e(r))+J(r)]n_m(r) \times\int_0^z \exp[-e\varphi(z')/T_e(r)]dz' \ , \quad (36)$$

where

$$J(r)=\frac{\bar{\alpha}b_{i\perp}}{e}\frac{1}{r}\frac{\partial}{\partial r}\left[r\frac{\partial T_e}{\partial r}\right] \ ,$$

$$J(0)=\frac{2\bar{\alpha}b_{i\perp}}{e}\left.\frac{\partial^2 T_e}{\partial r^2}\right|_{r=0} \ .$$

Equating Eqs. (30) and (36) at $r=0$, we obtain an integral equation for the potential $\varphi(z,0)$:

$$[\nu_i(T_{em})+J(0)]\int_0^z e^{-\eta(Z')}dZ'=[\nu_i(T_{em})+\nu_{ex}]\int_0^Z e^{-\eta(Z')}\exp\left\{-\int_{Z'}^Z \frac{dZ''}{[\eta(Z'')-\eta(Z')]^{1/2}}\right\}dZ' \ . \quad (37)$$

The solution of Eq. (37) give us the dependence T_{em} on L and $T_e''(0)$. We can rewrite Eq. (37) in the form

$$\int_0^Z e^{-\eta(Z')}dZ'=\mu(0)\int_0^Z e^{-\eta(Z')}\exp\left\{-\int_{Z'}^Z \frac{dZ''}{[\eta(Z'')-\eta(Z')]^{1/2}}\right\}dZ' \ , \quad (38)$$

where

$$\mu(0)=[\nu_i(T_{em})+\nu_{ex}]/[\nu_i(T_{em})+J(0)] \ . \quad (39)$$

We seek $\eta(Z)$ as a set of parabolic functions $\eta_k(Z)=A_kZ^2+B_kZ+C_k$, where $Z\supset[Z_{k-1},Z_k]$, $Z_k-Z_{k-1}=h$. The coefficients A_k, B_k, and C_k are to be selected from the conditions of continuity of $\eta(Z)$, $\eta'(Z)$ at Z_{k-1}:

$$\eta_k(Z_{k-1})=\eta_{k-1}(Z_{k-1}), \quad \eta_k'(Z_{k-1})=\eta_{k-1}'(Z_{k-1}) \ . \quad (40)$$

Instead of Eq. (38), we have

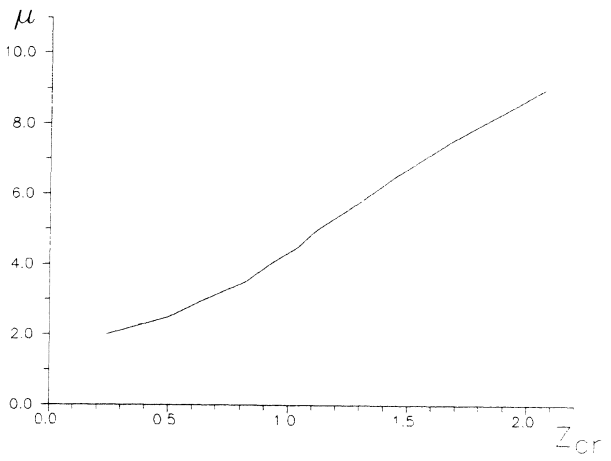

FIG. 2. Dependence of μ on Z_{cr} in dimensionless units.

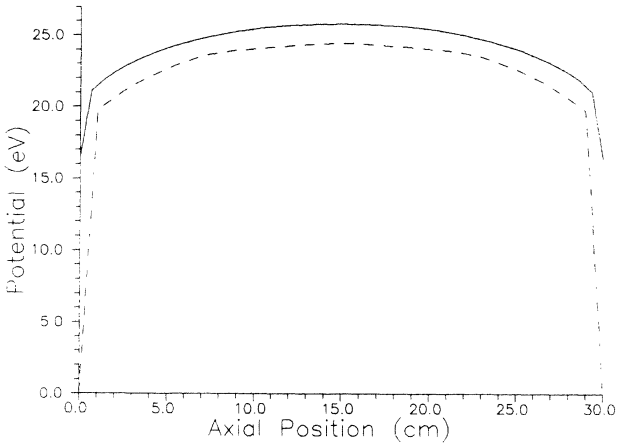

FIG. 5. The potential profile along the axis at $r=0$ as a function of longitudinal position.

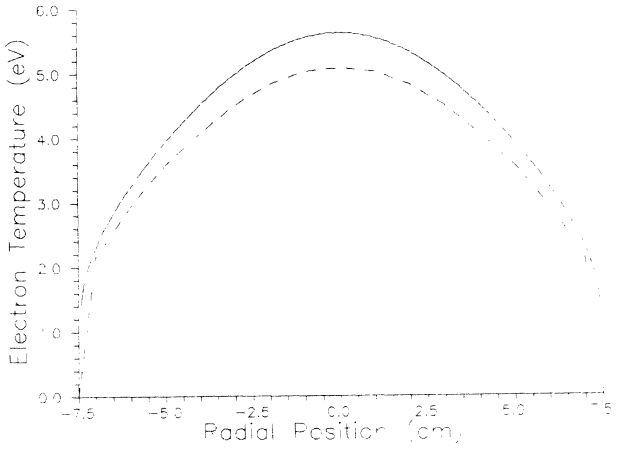

FIG. 3. The radial electron temperature profile at the axial midplane ($z=15$ cm). The solid and dashed lines in Figs. 3–7 represent theoretical results obtained in this paper and numerical results [1], respectively.

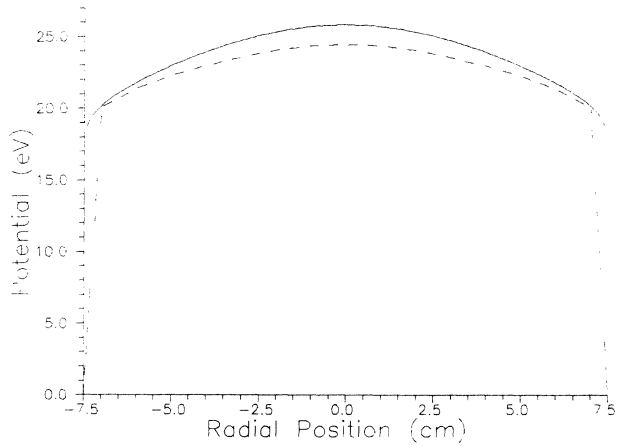

FIG. 6. The potential profile at the axial midplane as a function of radial position.

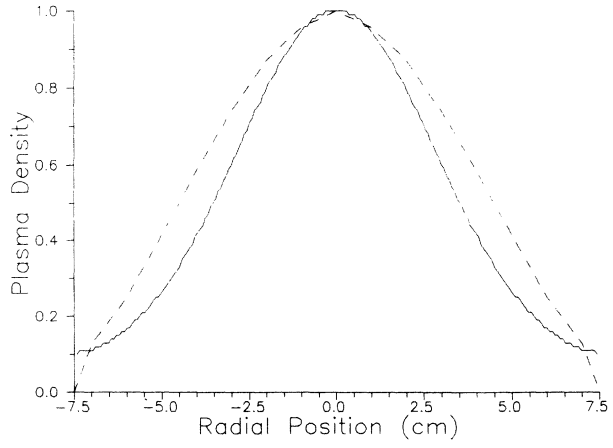

FIG. 4. The normalized radial plasma density profile at the axial midplane ($z=15$ cm) as a function of radial position.

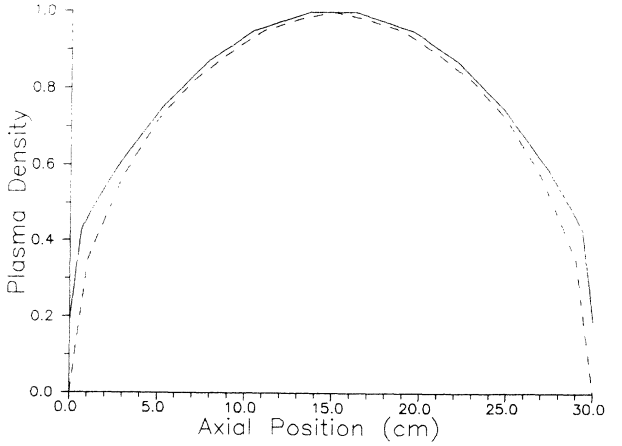

FIG. 7. The normalized plasma density as a function of axial position at $r=0$.

$$\int_0^{Z_k} e^{-\eta(Z')} dZ' = \mu(0) \int_0^{Z_k} e^{-\eta(Z')} \exp\left\{ - \int_{Z'}^{Z_k} \frac{dZ''}{[\eta(Z'') - \eta(Z')]^{1/2}} \right\} dZ' \ . \tag{41}$$

At $k=0$ we have $B_0 = C_0 = 0$, and A_0 can be easily found from Eq. (41). All the subsequent values A_k, B_k, and C_k are determined by Eqs. (40) and (41). Solutions of Eq. (38) are shown in Fig. 1. Using Fig. 2 and Eqs. (23), (32), and (39), we can obtain T_{em} for each value Z_{cr} for an arbitrary profile $T_e(r)$. Combining T_{em} obtained from Eqs. (23) and (39) for a Bessel-like profile of energy input [1], we obtain $T_e(r)$ profile (Fig. 3). For an arbitrary radius r, instead of Eq. (39), we have at $z = L/2$,

$$\mu(r) = [\nu_i(T_e(r)) + \nu_{ex}] \Big/ \left[\nu_i(T_e(r)) + \frac{\bar{\alpha} b_{i\perp}}{e} \frac{1}{r} \frac{\partial}{\partial r} \left[rn \frac{\partial T_e}{\partial r} \right] \Big/ n \right] \ . \tag{42}$$

From Eq. (42) we can obtain an expression for the density profile

$$n_m(r) = n_m(0) \exp \left[- \int_0^r \frac{\nu_i(r) - \dfrac{\nu_i(r) + \nu_{ex}}{\mu(r)} - J(r)}{\dfrac{\bar{\alpha} b_{i\perp}}{e} \dfrac{\partial T_e}{\partial r}} dr \right] \ . \tag{43}$$

The radial density profile is shown in Fig. 4. The axial and radial potential profiles obtained from Eq. (7) are presented in Figs. 5 and 6. The axial density profile can be obtained as $\exp[-\eta(z)]$ (see Fig. 7). The agreement with the results of [1] is quite satisfactory.

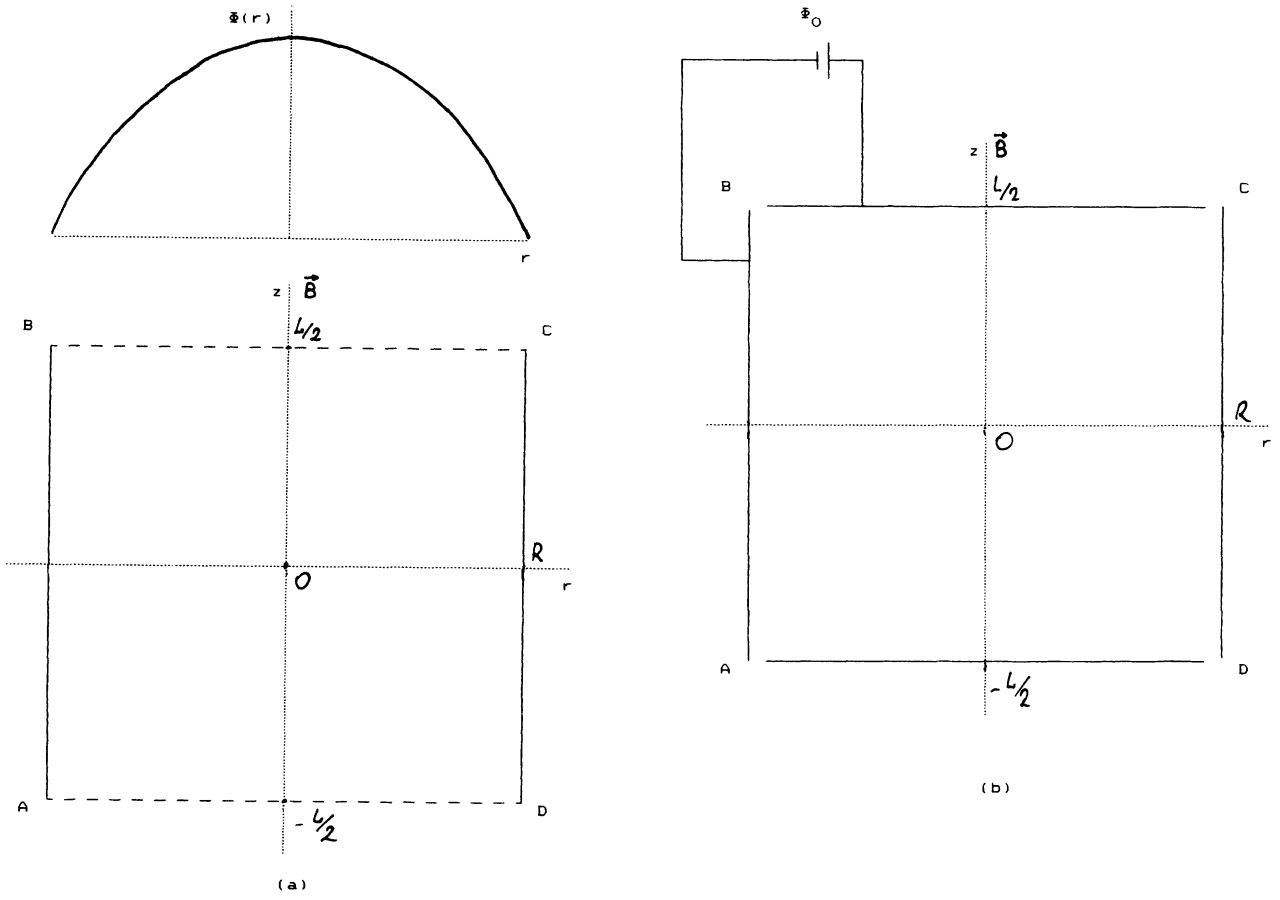

FIG. 8. Side view of the simulation domain: cylinder with length L and radius R. The uniform magnetic field is applied in the positive z direction. (a) The parts AD, BC of the vessel perpendicular to $\vec{B}$ are sectioned into concentric circular strips. The strips AD are under floating potential, and to the strips BC a monotonic potential profile $\Phi(r)$ is applied. (b) The potential difference Φ_0 is applied between the perpendicular and parallel (with respect to $\vec{B}$) walls AB and BC.

VI. CONTROL OF THE PLASMA PARAMETERS

A simple but very effective method of controlling plasma parameters based on our analysis can be suggested.

(1) According to Eq. (7), the plasma potential with respect to the end surfaces perpendicular to the magnetic field [*AD*,*BC* in Fig. 8(a)] is determined by the electron temperature only. So by applying to the wall *BC* that is perpendicular to $\vec{B}$ a radial potential profile $\Phi(r)$, as is shown in Fig. 8(a), we can control T_{em} and the density profile. This can be done by cutting the conducting walls *BC* and *AD* into thin insulated concentric strips. Equation (37) for the monotonic profile $\Phi(r)$ takes the form

$$\mu(L,T_{em})=[\nu_i(T_{em})+\nu_{ex}]/[\nu_i(T_{em})+2\Phi''(0)b_{i\perp}+J(0)] . \tag{44}$$

The increase of $|\Phi''(0)|$ leads to the increase of T_{em}.

(2) If the wall parallel to the magnetic field *AB* is biased negatively with respect to the end wall *BC*, as is shown in Fig. 8(b), the discharge remains unchanged, but all the potential difference is applied to the space-charge sheath adjacent to the side walls *DC*, *AB*. This enables one to control the energy of ions bombarding these walls.

(3) The applying of positive potential difference Φ_0 leads to a steep increase of the plasma density near the side walls *AB*,*CD* without changing the central part of the discharge.

VII. CONCLUSIONS

(1) An analytic model of the inhomogeneously heated magnetized plasma diffusion with $T_e \gg T_i$ in a conducting vessel is proposed.

(2) It is demonstrated that the radial potential profile is determined by the balance between the longitudinal electron escape to the vessel walls and ionization, and for the Maxwellian electron distribution is proportional to the electron temperature profile $T_e(r)$. In the general case the potential profile depends crucially on the electron kinetics.

(3) The plasma density profile is determined by the ion motion along and across the magnetic field. The plasma diffusion is accompanied by the current flow in the plasma volume. This current is short circuited by the conducting walls.

(4) The analytic results presented are in fair agreement with the numerical modeling.

(5) The plasma parameter profiles and intensities and the energy spectra of ion fluxes at the vessel surface are crucially dependent on the potential profile over the boundary surface. By varying this profile, its possible to control these important plasma characteristics.

ACKNOWLEDGMENT

The work was supported by the Russian Foundation of Fundamental Research, Grant Nos. 93-02-16905 and 94-02-04761.

[1] R. K. Porteous and D. B. Graves, IEEE Trans. Plasma Sci. **PS-19**, 204 (1991).

[2] A. P. Zhilinsky, V. A. Rozhansky, and L. D. Tsendin, Fiz. Plazmy **4**, 570 (1978) [Sov. J. Plasma Phys. **4**, 317 (1978)].

[3] A. P. Zhilinsky and L. D. Tsendin, Usp. Fiz. Nauk, **131**, 343 (1980) [Sov. Phys. Usp. **23**, 331 (1980)].

[4] V. A. Rozhansky and L. D. Tsendin, *Collisional Transport of a Partially Ionized Plasma* (in Russian) (Energoatomizdat, Moscow, 1988).

[5] A. Simon, Phys. Rev. **98**, 317 (1955).

[6] S. P. Voskoboinikov, I. Yu. Gurvich, and V. A. Rozhansky, Fiz. Plazmy **15**, 828 (1989) [Sov. J. Plasma Phys. **15**, 479 (1989)]; I. Yu. Gurvich and V. A. Rozhznsky (unpublished).

[7] A. P. Zhilinsky, I. F. Liventzeva, and L. D. Tsendin, Zh. Tekh. Fiz. **47**, 304 (1977) [Sov. Phys. Tech. Phys. **22**, 117 (1977)].